

1 **Contrasting short and long term**
2 **projections of the hydrological cycle**
3 **in the Southern extratropics**

4 YUTIAN WU *

Department of Earth, Atmospheric and Planetary Sciences, Purdue University

LORENZO M. POLVANI

*Department of Applied Physics and Applied Mathematics
and Department of Earth and Environmental Sciences,
Columbia University, New York, NY*

Submitted to J. Climate on January 12, 2015

Accepted by J. Climate on April 8, 2015

* *Corresponding author address:* Yutian Wu, Department of Earth, Atmospheric, and Planetary Sciences,
Purdue University, West Lafayette, IN, 47907
E-mail: wu640@purdue.edu

ABSTRACT

5

6 Analysis of model output from the Coupled Model Intercomparison Project, Phase 5
7 (CMIP5) reveals that, in the zonal mean, the near-term projections of summertime changes
8 of precipitation in the Southern Hemisphere (SH) subtropics are very widely scattered among
9 the models. As a consequence, over the next 50 years, the CMIP5 multimodel mean projects
10 no statistically significant trends in the SH subtropics in summer. This appears to be at
11 odds with the widely reported, and robust, poleward expansion of the subtropical dry zones
12 by the end of the 21st century.

13 This discrepancy between the shorter and longer term projections in SH summer, as
14 shown here, rests in the recovery of the ozone hole in the coming decades, as a consequence of
15 the Montreal Protocol. This is explicitly demonstrated by analyzing model experiments with
16 the Whole Atmosphere Community Climate Model, Version 4 (WACCM4), a high-top model
17 with interactive stratospheric chemistry, and coupled to land, ocean and sea ice components.
18 Contrasting WACCM4 integrations of the Representative Concentration Pathway 4.5 with
19 and without trends in surface concentrations of ozone depleting substances allows us to
20 demonstrate that stratospheric ozone recovery will largely offset the induced ‘wet gets wetter
21 and dry gets drier’ projections and the accompanying poleward expansion of the subtropical
22 dry zone in the SH. The lack of near-term statistically significant zonal mean changes in SH
23 hydrological cycle during summer is of obvious practical importance for many parts of the
24 world, and might also have implications for the Southern Ocean and the Antarctic continent.

1. Introduction

As anthropogenic greenhouse gases (GHG) continue to rise the hydrological cycle of the Earth is expected to change. Held and Soden (2006) originally proposed the ‘wet gets wetter and dry gets drier’ paradigm, which consists of a local intensification of the hydrological cycle accompanying global warming. Subsequent work by Seager et al. (2007, 2010) has emphasized that future changes of the hydrological cycle will also be affected by changes in the circulation, notably the poleward expansion of the subtropical dry zones (Lu et al. 2007) and the poleward shift of the midlatitude storm tracks (Yin 2005).

More recently, Scheff and Frierson (2012b) carefully investigated linear trends in precipitation – over the period 1980-2099 – as projected by the models participating in the Coupled Model Intercomparison Project, Phase 5 (CMIP5) under Representative Concentration Pathway (RCP) 8.5, the future scenario with greatest emission of greenhouse gases. They found that robust future precipitation declines are located, primarily, *poleward of the subtropical minimum* of the present-day precipitation climatology. This indicates a poleward expansion of the subtropical dry zones, which they found to be robust in the Southern Hemisphere over the entire seasonal cycle, confirming their earlier findings with the CMIP3 models, where they concluded that changes in extratropical precipitation, by the end of the 21st Century, can be characterized as ‘mostly midlatitude shifts’ (Scheff and Frierson 2012a).

In this paper, we turn our attention to shorter term projections, and focus on zonal-mean hydrological cycle changes in Southern Hemisphere (SH) summer in the next 50 years. In contrast to what has been reported in Scheff and Frierson (2012b), we show that in the coming half-century the zonal-mean projection of the precipitation changes in austral summer is not a poleward shift, as the CMIP5 models show no statistically significant shift in the SH in that season. Needless to say, the projection of such non-existent trends over a period lasting several decades into the future is of major practical importance.

To elucidate this lack of zonal mean trends in the coming decades, we perform modeling experiments of future projections with ozone depleting substances held fixed at current levels.

52 Using a stratosphere-resolving, chemistry-coupled, climate model, we demonstrate that the
53 lack of near-term changes in the SH hydrological cycle is a clear consequence of the Montreal
54 Protocol, which is expected to cause a substantial decrease in ozone depleting substances
55 and result in the closing of the ozone hole in the coming decades.

56 Our results build on the findings of a number of previous studies (Perlwitz et al. 2008;
57 Son et al. 2009; Polvani et al. 2011; McLandress et al. 2011; Arblaster et al. 2011; Barnes
58 et al. 2014), who have documented that the circulation changes induced by the closing of the
59 ozone hole will largely cancel the effects of increasing greenhouse gases in coming decades.
60 None of these previous studies, however, was specifically focused on the hydrological cycle
61 itself. We here construct a careful budget of the water cycle for the SH, and show that the
62 effect of the Montreal Protocol – via the recovery of the ozone hole – is largely dynamical in
63 character, rather than related to thermodynamics.

64 This paper is organized as follows. In Section 2 we describe the climate models and
65 the numerical experiments used in this study. In Section 3 we analyze the projections of
66 hydrological cycle changes in both the CMIP5 archive and experiments with and without
67 ozone recovery. The underlying mechanisms are also discussed in Section 3. A discussion in
68 Section 4 concludes the paper.

69 **2. Methods**

70 *a. The CMIP5 model output*

71 We start by contrasting the long and short term projections of the CMIP5 models (Taylor
72 et al. 2012). We analyze the future RCP4.5 and RCP8.5 scenario integrations (Meinshausen
73 and Coauthors 2011), where the total GHG radiative forcing reaches 4.5 and 8.5 W/m² at
74 the end of the 21st century, as well as historical integrations. All 24 CMIP5 models with
75 available monthly output of precipitation (P) and evaporation (E) are used here: they are
76 listed in Table 1. All these are atmosphere-ocean coupled models; however they comprise

77 a mix of well-resolved and poorly-resolved stratosphere components (Charlton-Perez et al.
78 2013). Also, the ozone concentrations in these models are specified in different ways: some of
79 models have interactive chemistry, while the majority simply read in the ozone concentrations
80 from precomputed values (see Eyring and Coauthors 2013, for more details).

81 While the CMIP5 integrations provide the latest and, presumably, most accurate version
82 of future projections of climate change in the presence of all known climate forcings, any
83 direct attribution of the projected changes to specific forcings is often difficult, especially
84 when the climate impacts of some of the forcings are of comparable magnitude but opposite
85 in sign. To understand the causes and mechanisms underlying climate projections, it is
86 often easier to use a single model in which individual forcings can be turned on and off,
87 rendering the attribution exercise relatively straightforward.

88 *b. The WACCM4 Experiments*

89 For the task of attribution, therefore, we use a specific model in which we specify single-
90 forcing changes. These were performed with the high-top configuration of Community Earth
91 System Model (CESM1): the Whole Atmosphere Community Climate Model, version 4
92 (WACCM4). WACCM4 is a stratosphere-resolving atmospheric model coupled to fully-
93 interactive stratospheric chemistry, land, ocean and sea ice components. WACCM4 is one of
94 the models that participated in the CMIP5 exercise, and the ‘historical’ CMIP5 simulations
95 with WACCM4 have been documented in detail in Marsh et al. (2013), which also contains
96 a full description of that model.

97 In this paper we analyze two sets of WACCM4 integrations. The first set is an ensemble
98 of three RCP4.5 model runs, performed followed the standard CMIP5 specifications for
99 RCP4.5 pathway, between 2001 and 2065. The second set consists of three integrations
100 identical to those in the first set in every respect, except for the surface concentrations of
101 ozone depleting substances (ODS): the latter are held fixed at year 2000 values. We refer to
102 these two 3-member ensembles as two “experiments”.

103 In the first experiment, labeled simply ‘RCP4.5’, stratospheric ozone over the Antarctic
104 polar cap is fully recovered by 2065 as one can see, for instance, in Fig. 1a of Smith et al.
105 (2012) where the same runs were analyzed. In the second experiment, ozone concentrations at
106 2065 are nearly identical to those in the year 2000. Since increasing greenhouse gases are the
107 major forcing in this second experiment, we label it ‘GHG \uparrow ’. In many figures below, we also
108 plot the difference between the two experiments: this is labeled ‘ODS \downarrow ’, as ODS are the only
109 forcing that has been changed between the two experiments. Note that while stratospheric
110 ozone is the primary driver of the circulation changes seen in the difference plots, ‘ODS \downarrow ’ is
111 the proper way to label the difference, not ‘ozone \uparrow ’, since ozone is interactively computed
112 in WACCM4: surface ODS are the external forcing. Moreover, ODS are the substances
113 actually regulated by the Montreal Protocol, not ozone itself.

114 Lastly, for the sake of completeness, a couple of technical notes. One: the domain of
115 interest here is the SH, between 70°S and 30°S. Two: for all variables, statistical significance
116 is evaluated via a simple Student’s t test, using the 90% confidence interval. Three: in order
117 to accurately calculate latitudinal shifts of zonal mean profiles, climate variables are first
118 interpolated onto a 0.1° grid using a cubic spline interpolation.

119 **3. Results**

120 *a. CMIP5 Hydrological Cycle Projections*

121 We start by reproducing the results of Scheff and Frierson (2012b) and, in Fig. 1a, show
122 the future projection of precipitation (P) in an ensemble of CMIP5 models in the RCP8.5
123 scenario in austral summer during 2001-2099 (red line). The curves are here calculated as
124 the sum of the recent climatology (defined as the 1981-2000 average) plus the linear trends
125 in the future simulations from 2001 to 2099. Compared to the climatology (thin black
126 line) the future projection of P is well separated. Note also that the projection is robust
127 across all latitudes at the 90% level, with a significant wetting trend at mid-to-high latitudes

128 (poleward of 50°S) and a drying trend poleward of the subtropical minimum (50°-40°S).
129 The precipitation decline poleward of subtropical minimum (roughly between 37° and 47°S)
130 results, therefore, in a poleward shift, as reported by Scheff and Frierson (2012a,b).

131 The point of this paper, however, is that this shift disappears when one considers shorter
132 term projections. Consider, in particular, the projection for the shorter period 2001-2065: it
133 is shown in Fig. 1b for some CMIP5 model simulations. Despite the statistically significant
134 wetting trend at mid-to-high latitudes, the drying trend in the subtropical region (between
135 50° and 30°S) is no longer robust among CMIP5 models. A similarly insignificant projection
136 is found for the RCP4.5 scenario, is shown in Fig. 1c. The agreement between the two
137 scenarios is not surprising, since the forcings are not very different by the year 2065.

138 Since the global distribution of precipitation minus evaporation ($P - E$) better captures
139 the entire hydrological cycle, we show in Fig. 2a the future projection of $P - E$ under RCP8.5
140 during 2001-2099, again in the CMIP5 models. As for P alone, the future projection of $P - E$
141 is also well separated from its climatology by the end of the century, with a large wetting
142 trend poleward of 50°S and a drying trend equatorward of about 50°S. One difference between
143 Fig. 1a and Fig. 2a is seen around 30°S, where the E increases more than P .

144 The actual value of the latitudinal shift of the subtropical dry zone edge for each model,
145 i.e. the zero crossing of $P - E$, is shown in the inset plot of Fig. 2a. As one can see, the
146 subtropical dry zone edge shifts poleward by about 1° latitude in multi-model mean, and this
147 poleward expansion is highly robust among the CMIP5 models: not a single model shows
148 an equatorward shift.

149 For the shorter period 2001-2065, Fig. 2b shows the $P - E$ projections for the same
150 simulations. Comparing these to Fig. 1b, we note that the $P - E$ reduction is statistically
151 significant in most of the subtropical region: this is due to the robust increase of E there.
152 More importantly, in contrast to Fig. 2a, the latitudinal shift of the subtropical dry zone edge
153 is no longer statistically significant, and is more widely spread across the CMIP5 models.
154 Furthermore, a latitudinal shift of the subtropical dry zone edge is also absent in the RCP4.5

155 simulations, shown in Fig. 2c, over the period of ozone recovery. Similar findings of near
156 zero trends in the SH summer in coming decades have been reported in Barnes et al. (2014).
157 The question, at this point, becomes: why is the shift missing in the short term projections?

158 *b. WACCM4 Hydrological Cycle Projections: the role of ODS*

159 To attribute the missing shift of the SH subtropical dry zone edge in the coming decades
160 directly to the Montreal Protocol, which controls ODS, we next turn to the single forcing
161 experiments with WACCM4. Consider first, the zonal mean $P - E$ linear trend over the
162 period 2001-2065 from the RCP4.5 integrations of WACCM4, shown in Fig. 3a. Note that
163 we here plot the trend, not the projection, as in the previous two figures; this is done to
164 bring out the response to applied forcings. In Fig. 3a, one clearly sees a wetting trend
165 at mid-to-high latitudes poleward of 50°S and a drying trend equatorward of 50°S in the
166 ensemble mean WACCM4 runs (thick red line). See also the good agreement between the
167 individual ensemble members (thin red lines), which yields a statistically significant trend.
168 Our WACCM4 results, also, are in good general agreement with the CMIP5 multi-model
169 mean (blue curve), in both pattern and magnitude. And, as for the CMIP5, the latitudinal
170 shift of the subtropical dry zone edge is statistically insignificant in WACCM4 (not shown).

171 Now we separate the hydrological cycle response into the one due to GHG increase and
172 the one resulting from decreasing ODS (and the accompanying ozone recovery). In Fig. 3b
173 we show the hydrological cycle response in the GHG↑ experiment, where ODS are kept fixed.
174 See how the trends in that case are noticeably different from the RCP4.5 case. For the GHG↑
175 case, WACCM4 projects a moistening trend poleward of 55°S and a drying trend between
176 55° and 35°S: this results in a clear poleward shift of the hydrological cycle.

177 The difference between the RCP4.5 and GHG↑ experiments can be seen in Fig. 3c. The
178 response to decreasing ODS consists of a wetting trend in the midlatitudes between 60°
179 and 40°S, and a drying trend in both the subtropics (between 40° and 30°S, though not
180 statistically significant) and high latitudes (poleward of 60°S). Note that, the magnitude

181 of the response in the ODS \downarrow case is similar in magnitude but *opposite* in sign to that of
182 GHG \uparrow . This ODS \downarrow response is also similar in pattern, but opposite in sign, to the one
183 shown reported in Polvani et al. (2011) (see their Fig. 11) and Kang et al. (2011) (see
184 their Fig. 3) for period stratospheric ozone depletion (roughly 1960-2000), when the ODS
185 forcing is of opposite sign. In other seasons, the difference between the RCP4.5 and GHG \uparrow
186 experiments becomes negligible (not shown), as one would expect if ozone recovery is the
187 primary forcing canceling the effect of increased GHG.

188 In summary then: the future response of the hydrological cycle in austral summer will
189 depend very sensitively on both the GHG increase and stratospheric ozone recovery, which
190 tend to offset each other. With the anticipated recovery of Antarctic ozone hole, the wetting
191 trend polewards of 60°S will be greatly reduced: this might have implications for the Southern
192 Ocean (e.g., Durack et al. 2012) and the Antarctic continent. Furthermore, the significant
193 poleward expansion of the subtropical dry zone associated with anthropogenic GHG increase
194 will also largely mitigated by the dry zone contraction due to stratospheric ozone recovery,
195 leading to an insignificant position change of the hydrological cycle in the future. A more
196 detailed understanding of the absence of shifts in the hydrological cycle in SH summer over
197 the next several decades is discussed next.

198 *c. Dynamical Mechanisms Associated With Hydrological Cycle Projections*

199 A quantitative evaluation of the mechanisms associated with the hydrological cycle re-
200 sponse can be obtained by performing a complete moisture budget analysis, along the lines of
201 Seager et al. (2007, 2010). The moisture budget analysis separates the response of $P - E$ into
202 the contributions from the thermodynamic (TH), the mean circulation dynamical (MCD)

203 and the transient eddy (TE) components. It is written as:

$$204 \quad \delta \langle \overline{P - E} \rangle \approx \delta \text{TH} + \delta \text{MCD} + \delta \text{TE} \quad (1)$$

$$205 \quad \delta \text{TH} = -\frac{1}{ag\rho_w} \frac{1}{\cos \phi} \frac{\partial}{\partial \phi} \left\langle \int_0^{p_s} \bar{v} \cdot \delta \bar{q} dp \right\rangle \cos \phi \quad (2)$$

$$206 \quad \delta \text{MCD} = -\frac{1}{ag\rho_w} \frac{1}{\cos \phi} \frac{\partial}{\partial \phi} \left\langle \int_0^{p_s} \delta \bar{v} \cdot \bar{q} dp \right\rangle \cos \phi \quad (3)$$

$$207 \quad \delta \text{TE} = -\frac{1}{ag\rho_w} \frac{1}{\cos \phi} \frac{\partial}{\partial \phi} \left\langle \int_0^{p_s} \delta \overline{v'q'} dp \right\rangle \cos \phi \quad (4)$$

208 where bars denote monthly averages, primes denote deviations from monthly averages and
 209 brackets indicate zonal averages. The TH term identifies the change in zonal mean specific
 210 humidity (q), the MCD term tracks the response in zonal mean circulation, and the TE term
 211 isolates the change in poleward moisture transport associated with transient eddies.

212 These individual components, as they contribute to the linear trends from 2001 to 2065 in
 213 the WACCM4 experiments, are shown in Fig. 4. To keep the figures readable, we only show
 214 the ensemble mean of 3 integrations in each panel. Note first that for all three cases (RCP4.5,
 215 GHG \uparrow and ODS \downarrow), the sum of the TH, MCD and TE terms, denoted by the ‘moisture flux
 216 conv’ (dashed-dotted red lines), reproduces very well the $P - E$ modeled trends (solid red
 217 lines). This confirms the usefulness of the analysis to clarify the underlying mechanism.

218 Let us start by considering the RCP4.5 decomposition of the SH water cycle response,
 219 shown with Fig. 4a. The response of $P - E$ consists of an intensification in the middle and
 220 high latitudes, say southward of 47°S, and a reduction at lower latitudes. From the budget
 221 analysis, it is clear that the transient eddy moisture flux (green line) is the largest of the
 222 three components. The mean circulation and thermodynamic terms also play some role.

223 In response to GHG increase, shown in Fig. 4b, the poleward shift of $P - E$ is again
 224 due, mostly, to a shift and intensification of transient eddy moisture flux. Interestingly, the
 225 thermodynamic component makes only a minor contribution to the intensification of the
 226 hydrological cycle, as does the the mean circulation. The key role of transient eddies has
 227 already been noted, e.g. by Seager et al. (2010).

228 In response to decreasing ODS, as seen in Fig. 4c, the change in $P - E$ is a near mirror

229 image of the one for GHG \uparrow case. Furthermore, the decline in $P - E$ at high latitudes in the
 230 ODS \downarrow case is caused, equally, by changes in the mean circulation and transient eddies. In
 231 other words, the cancellation of future changes in the hydrological cycle is almost entirely
 232 dynamical, not thermodynamical¹, in origin.

233 Finally, we compute actual values for the latitudinal shift of the hydrological cycle in the
 234 WACCM4 integrations, together with the specific contributions from the dynamics including
 235 the expansion/contraction of the zonal mean circulation and the poleward/equatorward shift
 236 of the moisture flux associated with transient eddies. Following Lu et al. (2010), we compute
 237 the latitudinal shift of a bell-shaped climate variable, X , using the expression:

$$238 \quad \delta\phi = \frac{X_{r,\max}}{X_{p,\max}}(\delta X^+ - \delta X^-)\left(\frac{dX_r^-}{d\phi} - \frac{dX_r^+}{d\phi}\right)^{-1} \quad (5)$$

239 where $\delta\phi$ denotes the latitudinal shift, r and p denote reference state and perturbed state,
 240 respectively, the superscripts $+$ and $-$ denote the polar flank and the equatorward flank of
 241 the climate variable X , and $\delta X^+ = X_p^+ - X_r^+$ and $\delta X^- = X_p^- - X_r^-$. A detailed derivation
 242 (5) can be found in Lu et al. (2010). This method measures the shift of the whole pattern
 243 of the climate variable X by making use of the dipolar structure of the response on the
 244 equatorward and poleward flanks, as well as the change in the magnitude of X .

245 We here compute the shift in three variables. The first, obviously, is $P - E$, for which we
 246 choose the latitudinal bands of $+$ and $-$ as $80^\circ - 60^\circ\text{S}$ and $60^\circ - 40^\circ\text{S}$, centered around 60°S
 247 where the climatological maximum is located. Second, we compute the shift of the zonal
 248 mean streamfunction Ψ maximum at 500 mb, with bands $70^\circ - 50^\circ\text{S}$ and $50^\circ - 30^\circ\text{S}$ chosen
 249 for the poleward and equatorward flank respectively, and centered around 50°S , where Ψ
 250 is maximal in the climatology. This variable denotes a shift in the Farrell cell. The same
 251 parameters are chosen for the third variable: the eddy moisture flux $\langle \overline{v'q'} \rangle$ at 700 mb. Results

¹The thoughtful reader may have noticed that the transient eddy term TE, as defined in Eq. (4), also involves changes in specific humidity (q'), and hence it might be inappropriate to call this term a dynamical contribution. However, the changes in specific humidity resulting from stratospheric ozone forcing are usually very small, and it is through v' that the response to the forcing is realized.

252 are not sensitive to specific choices for the bands.

253 Fig. 5 shows the latitudinal shift of the hydrological cycle, the zonal mean circulation,
254 and the transient eddy moisture flux in the WACCM4 integrations. Clearly, over the period
255 2001-2065, there is no statistically significant shift of the hydrological cycle in the RCP4.5
256 experiment (black crosses). Furthermore, it is crystal clear that the absence of $P - E$ shifts
257 is caused by the large cancellation between increasing greenhouse gases (red) – producing
258 a poleward shift of about 0.5° in ensemble average – and the comparable equatorward shift
259 due to decreasing ODS (and the accompanying recovery of stratospheric ozone).

260 In terms of mechanisms, this cancellation in the shift of the hydrological cycle comes,
261 largely, from changes in the mean circulation and transient eddies, not the thermodynamics.
262 While the Ferrel cell tends to move poleward in response to greenhouse warming (about
263 0.3° poleward in ensemble mean), the recovery of ozone shifts the zonal mean circulation in
264 the midlatitudes equatorward by about 0.5° latitude in ensemble average. In the WACCM4
265 RCP4.5 simulations, the Ferrel cell moves slightly equatorward, due to the shift on the polar
266 flank but we find no shift on the equatorward flank (which corresponds to the southern edge
267 of the Hadley cell, not shown). The near cancellation is also seen in the moisture trans-
268 port associated with the transient eddies despite a larger ensemble spread for the RCP4.5
269 experiment.

270 4. Conclusion

271 We have shown that there exists a marked difference between the short and long term
272 predictions of changes in the zonal mean precipitation, in SH summer subtropics, in the
273 CMIP5 models. In a nutshell, the robust projections of midlatitude shifts that have been
274 reported in the literature are not seen until the very end of the 21st Century and, for the
275 next 50 years, no significant zonal mean trends are projected in that season in the SH.

276 Confirming earlier studies reviewed in the Introduction, and with the help of new single-

277 forcing integrations with WACCM4, a stratosphere-resolving model with interactive ozone
278 chemistry, we have demonstrated that the decreased concentration of ODS (resulting in the
279 closing of the ozone hole in the next several decades) is the key anthropogenic forcing that
280 will cancel the GHG induced poleward shift in the water cycle. In essence, therefore, the
281 Montreal Protocol will result in a substantial mitigation of climate change, in the sense of a
282 multi-decadal long delay in the emergence of the effects of GHG, in SH summer.

283 One might be tempted to argue that the climate impacts of the Montreal Protocol will
284 be relatively small, as they will be confined to a single season. Such an argument, however,
285 is simplistic. First, recall that summer is the rainy season in most parts of the Southern
286 Hemisphere, notably South America, South Africa and Eastern Australia. Second, note that
287 while the findings here are uniquely focused on the zonal mean, there is reason to believe
288 that the impact of the Montreal Protocol will be keenly felt in specific regions.

289 A clear example is offered by the region known as South Eastern South America (SESA),
290 which has experienced the world's largest increase in precipitation in the late 20th Century.
291 As shown in Gonzalez et al. (2014), the formation of the ozone hole in the late decades of
292 the 20th Century has been a key driver of those observed precipitation increases. Hence, as
293 the ozone hole closes in the coming decades, there is every reason to expect that the recent
294 precipitation increases will be greatly reduced, and possibly reversed.

295 Keeping in mind that we only have 3 ensemble members at our disposal, and that the
296 version of WACCM used here has a relatively coarse horizontal resolution (1.9° in latitude
297 and 2.5° in longitude), we nonetheless attempt to offer a glimpse of how *on regional scales* the
298 recovery of stratospheric ozone in the coming decades might offset the impact of increasing
299 greenhouse gases on the hydrological cycle. In Fig. 6, we plot the 2001-2065 DJF trends in
300 $P - E$, for four regions of interest (Australia, SESA, New Zealand and Tasmania); the top
301 row shows the response to increasing GHG, and the bottom row the response to decreasing
302 ODS. While there is little statistical significance beyond some parts of Australia and possibly
303 SESA, we draw the reader's attention to a simple fact: the colors in the top and bottom

304 rows are clearly reversed, indicating that the trends associated with ODS and GHG forcings
305 are basically opposite in sign – and this happens in all four regions. Of course this is merely
306 impressionistic, and any conclusions from a single model need to be taken with extreme
307 caution. That said, Fig. 6 does suggest that the ODS/GHG cancellation might actually
308 be observable in some populated areas of the Southern Hemisphere, although we leave a
309 thorough study of any given region for future papers.

310 Finally, a note about internal variability. As the hydrological cycle in SH summer will
311 be driven, in the short term, by two large yet opposing anthropogenic forcings (increasing
312 GHG and decreasing ODS), the role of internal climate variability will be larger than what
313 it otherwise would be. While the CMIP5 multi-model mean shows a non-existent trend, it is
314 entirely possible that either positive or negative trends will actually occur. Hence, while the
315 Montreal Protocol might be said to result in a mitigation of the effect of increasing GHG in
316 the near future, it also renders climate projections more uncertain than they would otherwise
317 be.

318 *Acknowledgments.*

319 The authors acknowledge the help of Dr. Haibo Liu for obtaining the CMIP5 data, and
320 thank Dr. Jack Scheff for several useful comments on an earlier draft of the paper. The
321 authors acknowledge the World Climate Research Programme’s Working Group on Coupled
322 Modelling, which is responsible for CMIP, and we thank the climate modeling groups (listed
323 in Table 1 of this paper) for producing and making available their model output. For CMIP
324 the U.S. Department of Energy’s Program for Climate Model Diagnosis and Intercomparison
325 provides coordinating support and led development of software infrastructure in partnership
326 with the Global Organization for Earth System Science Portals. YW is supported by a
327 startup fund from the Department of Earth, Atmospheric, and Planetary Sciences at Purdue
328 University. LMP is supported by a grant from the US National Science Foundation.

REFERENCES

- 331 Arblaster, J. M., G. A. Meehl, and D. J. Karoly, 2011: Future climate change in the Southern
332 Hemisphere: Competing effects of ozone and greenhouse gases. *Geophys. Res. Lett.*, **38**,
333 L02701, doi:10.1029/2010GL045384.
- 334 Barnes, E. A., N. W. Barnes, and L. M. Polvani, 2014: Delayed Southern Hemisphere climate
335 change induced by stratospheric ozone recovery, as projected by the CMIP5 models. *J.*
336 *Clim.*, **27**, 852–867.
- 337 Charlton-Perez, A. J., et al., 2013: On the lack of stratospheric dynamical variability in low-
338 top versions of the CMIP5 models. *J. Geophys. Res.*, **118**, 1–12, doi:10.1002/jgrd.50125.
- 339 Durack, P. J., S. E. Wijffels, and R. J. Matear, 2012: Ocean salinities reveal strong global
340 water cycle intensification during 1950 to 2000. *Sci.*, **336**, 455–458, doi: 10.1126/sci-
341 ence.1212222.
- 342 Eyring, V. and Coauthors, 2013: Long-term ozone changes and associated climate impacts
343 in CMIP5 simulations. *J. Geophys. Res.*, **118**, 5029–5060.
- 344 Gonzalez, P., L. Polvani, R. Seager, and G. Correa, 2014: Stratospheric ozone depletion: a
345 key driver of recent precipitation trends in South Eastern South America. *Clim. Dyn.*, **42**,
346 1775–1792.
- 347 Held, I. M. and B. J. Soden, 2006: Robust response of the hydrological cycle to global
348 warming. *J. Clim.*, **19**, 5686–5699.
- 349 Kang, S., L. M. Polvani, J. C. Fyfe, and M. Sigmond, 2011: Impact of polar ozone depletion
350 on subtropical precipitation. *Sci.*, **332**, 951–954.

351 Lu, J., G. Chen, and D. M. W. Frierson, 2010: The position of the midlatitude storm track
352 and eddy-driven westerlies in aquaplanet AGCMs. *J. Atmos. Sci.*, **67**, 3984–4000.

353 Lu, J., G. A. Vecchi, and T. Reichler, 2007: Expansion of the Hadley cell under global
354 warming. *Geophys. Res. Lett.*, **34**, L06 805, doi:10.1029/2006GL028 443.

355 Marsh, D. R., M. J. Mills, D. E. Kinnison, J.-F. Lamarque, N. Calvo, and L. M. Polvani,
356 2013: Climate change from 1850 to 2005 simulated in CESM1(WACCM). *J. Clim.*, **26**,
357 7372–7391.

358 McLandress, C., T. G. Shepherd, J. F. Scinocca, D. A. Plummer, M. Sigmond, A. I. Jonsson,
359 and M. C. Reader, 2011: Separating the dynamical effects of climate change and ozone
360 depletion. Part II: Southern Hemisphere troposphere. *J. Clim.*, **24**, 1850–1868.

361 Meinshausen, M. and Coauthors, 2011: The RCP greenhouse gas concentrations and their
362 extensions from 1765 to 2300. *Climatic Change*, **109**, 213–241.

363 Perlwitz, J., S. Pawson, R. L. Fogt, J. E. Nielsen, and W. D. Neff, 2008: Impact of
364 stratospheric ozone hole recovery on Antarctic climate. *Geophys. Res. Lett.*, **35**, L08 714,
365 doi:10.1029/2008GL033 317.

366 Polvani, L. M., M. Previdi, and C. Deser, 2011: Large cancellation, due to ozone recovery,
367 of future Southern Hemisphere atmospheric circulation trends. *Geophys. Res. Lett.*, **38**,
368 L04 707, doi:10.1029/2011GL046 712.

369 Scheff, J. and D. Frierson, 2012a: 21st-century multi-model subtropical precipitation declines
370 are mostly mid-latitude shifts. *J. Clim.*, **25**, 4330–4347.

371 Scheff, J. and D. Frierson, 2012b: Robust future precipitation declines in CMIP5 largely
372 reflect the poleward expansion of model subtropical dry zones. *Geophys. Res. Lett.*, **39**,
373 L18 704, doi: 10.1029/2012GL05 910.

- 374 Seager, R., N. Naik, and G. A. Vecchi, 2010: Thermodynamic and dynamic mechanisms
375 for large-scale changes in the hydrological cycle in response to global warming. *J. Clim.*,
376 **23(17)**, 4651–4668.
- 377 Seager, R., et al., 2007: Model projections of an imminent transition to a more arid climate
378 in southwestern North America. *Sci.*, **316(5828)**, 1181–1184.
- 379 Smith, K. M., L. M. Polvani, and D. R. Marsh, 2012: Mitigation of 21st century
380 Antarctic sea ice loss by stratospheric ozone recovery. *Geophys. Res. Lett.*, **39**, L20 701,
381 doi:10.1029/2012GL053 325.
- 382 Son, S.-W., N. Tandon, P. L.M., and D. Waugh, 2009: Ozone hole and southern hemisphere
383 climate change. *Geophys. Res. Lett.*, **35**, L15 705, doi:10.1029/2009GL038 671.
- 384 Taylor, K. E., R. J. Stouffer, and G. A. Meehl, 2012: An overview of CMIP5 and the
385 experiment design. *Bull. Amer. Meteor. Soc.*, **93**, doi:10.1175/BAMS-D-11-00 094.1.
- 386 Yin, J. H., 2005: A consistent poleward shift of the storm tracks in simulations of 21st
387 century climate. *Geophys. Res. Lett.*, **32**, L18 701, doi:10.1029/2005GL023 684.

388 **List of Tables**

389 1 The 24 CMIP5 models used in this study with information on host institute
390 and atmospheric model resolution (L refers to number of vertical levels, T to
391 triangular truncation and C to cubed sphere). 19

TABLE 1. The 24 CMIP5 models used in this study with information on host institute and atmospheric model resolution (L refers to number of vertical levels, T to triangular truncation and C to cubed sphere).

Institute	Model Name	Atmospheric Resolution (lon \times lat) level
Commonwealth Scientific and Industrial Research Organisation (CSIRO), Australia, and Bureau of Meteorology (BOM), Australia	1. ACCESS1-0	N96 (1.875° \times 1.25°) L38
	2. ACCESS1-3	N96 L38
Beijing Climate Center, China Meteorological Administration	3. bcc-csm1-1	T42 (2.8125° \times 2.8125°) L26
Canadian Centre for Climate Modelling and Analysis	4. CanESM2	T63 (1.875° \times 1.875°) L35
National Center for Atmospheric Research (NCAR)	5. CCSM4	288 \times 200 (1.25° \times 0.9°) L26
Centre National de Recherches Meteorologiques / Centre Europeen de Recherche et Formation Avancees en Calcul Scientifique	6. CNRM-CM5	T127 (1.4° \times 1.4°) L31
Commonwealth Scientific and Industrial Research Organisation in collaboration with the Queensland Climate Change Centre of Excellence	7. CSIRO-Mk3.6.0	T63 L18
The First Institute of Oceanography, SOA, China Geophysical Fluid Dynamics Laboratory (NOAA GFDL)	8. FIO-ESM	T42 L26
	9. GFDL-CM3	C48 (2.5° \times 2.0°) L48
	10. GFDL-ESM2G	144 \times 90 (2.5° \times 2.0°) L24
NASA Goddard Institute for Space Studies (GISS)	11. GFDL-ESM2M	144 \times 90 L24
	12. GISS-E2-R	144 \times 90 L40
Met Office Hadley Centre (HadGEM2-ES contributed by Instituto Nacional de Pesquisas Espaciais)	13. HadGEM2-CC	192 \times 144 (1.25° \times 1.875°) L60
	14. HadGEM2-ES	N96 L38
Institute for Numerical Mathematics	15. inmcm4	180 \times 120 (2.0° \times 1.5°) L21
Institut Pierre-Simon Laplace (IPSL)	16. IPSL-CM5A-LR	96 \times 96 (3.75° \times 1.875°) L39
	17. IPSL-CM5A-MR	144 \times 143 (2.5° \times 1.25°) L39
	18. IPSL-CM5B-LR	96 \times 96 L39
Japan Agency for Marine-Earth Science and Technology, Atmosphere and Ocean Research Institute (The University of Tokyo), and National Institute for Environmental Studies	19. MIROC-ESM	T42 L80
	20. MIROC-ESM-CHEM	T42 L80
	21. MIROC5	T85 (1.41° \times 1.41°) L40
Max Planck Institute for Meteorology (MPI-M)	22. MPI-ESM-LR	T63 L47
Meteorological Research Institute	23. MRI-CGCM3	T159 (1.125° \times 1.125°) L48
Norwegian Climate Centre	24. NorESM1-M	144 \times 96 (2.5° \times 1.875°) L26

392 List of Figures

- 393 1 The future projection of precipitation (P) in austral summer (DJF) for CMIP5
394 (a) RCP8.5 during 2001-2099, (b) RCP8.5 during 2001-2065, and (c) RCP4.5
395 during 2001-2065. The climatology, plotted in black, is the CMIP5 multi-
396 model average of 1981-2000 from the historical runs and the future projection
397 in (a), plotted in thick red, is the sum of the climatology and the linear
398 response from 2001 to 2099 in the RCP8.5 scenario, similarly for (b)(c). Sta-
399 tistically significant responses at the 90% level, are circled. 22
- 400 2 Same as Fig. 1 except for precipitation minus evaporation ($P - E$). In the inset
401 plot, the latitudinal shift of the subtropical dry zone edge, which is measured
402 by the zero crossing of $P - E$, is plotted in red cross for each model and in
403 thick black cross for multi-model average. Bar shows one standard deviation
404 of the multi-model results. 23
- 405 3 The linear trend in zonal mean $P - E$ in austral summer (DJF) during 2001-
406 2065 for (a) the RCP4.5 scenario, (b) GHG \uparrow experiment, and (c) ODS \downarrow exper-
407 iment from the WACCM4 integrations. Thin black line shows the climatology
408 of $P - E$ during 1981-2000 from the WACCM4 historical integrations, divided
409 by a factor of 10. Thick red line shows the linear trend of $P - E$ during 2001-
410 2065 in average of three ensemble runs and thin red line shows the response
411 from individual run. Thick blue line shows the CMIP5 multi-model averages
412 during 2001-2065. Statistically significant responses, at the 90% level, are
413 circled. 24

- 414 4 The WACCM4 moisture budget analysis for the linear trend in zonal mean
415 $P - E$ in DJF for (a) the RCP4.5 scenario, (b) GHG \uparrow experiment, and (c)
416 ODS \downarrow experiment. The 1981-2000 average of $P - E$, divided by a factor
417 of 10, is plotted in thin black as a reference for climatology, and the linear
418 trend of $P - E$ during 2001-2065 is plotted in thick red. The sum of the
419 thermodynamic (magenta), mean circulation dynamic (blue), and transient
420 eddy moisture flux convergence (green) components is denoted by 'moisture
421 flux conv' and is plotted in thick dashed-dotted red line. 25
- 422 5 The latitudinal shift of $P - E$, the Ferrel cell and the transient eddy moisture
423 flux in DJF during 2001-2065. Black indicated the RCP4.5 scenario, red
424 the GHG \uparrow experiment, and blue the ODS \downarrow experiment. Large crosses show
425 ensemble averages; small crosses show individual ensemble members; bars
426 show one standard deviation for each ensemble. 26
- 427 6 The linear trend in $P - E$ (in unit of [mm/day]) in DJF during 2001-2065
428 in (a)(e) Australia, (b)(f) South Eastern South America (SESA), (c)(g) New
429 Zealand, and (d)(h) Tasmania in the GHG \uparrow (top) and ODS \downarrow (bottom) exper-
430 iments. Statistically significant responses, at the 90% level, are dotted. 27

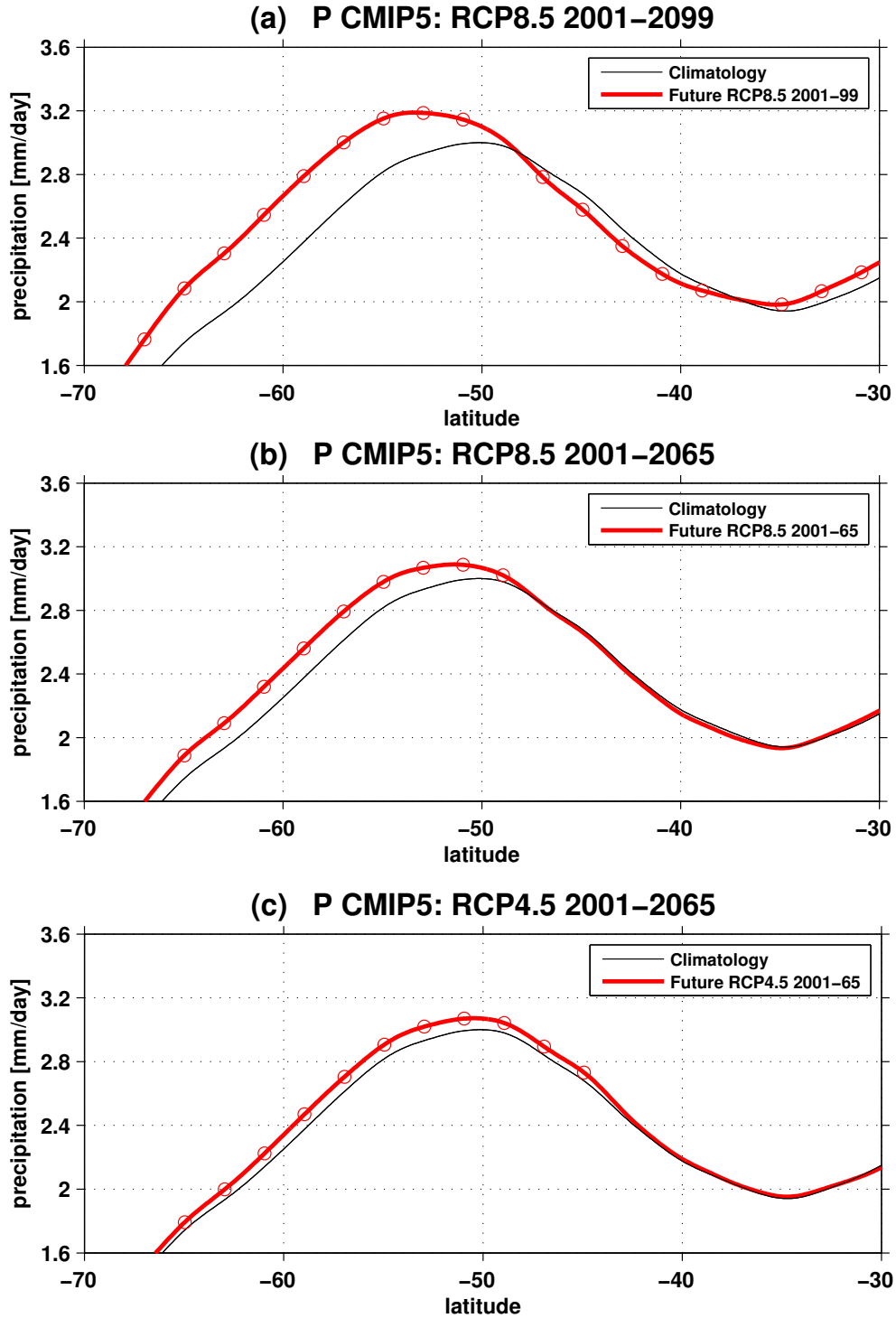


FIG. 1. The future projection of precipitation (P) in austral summer (DJF) for CMIP5 (a) RCP8.5 during 2001-2099, (b) RCP8.5 during 2001-2065, and (c) RCP4.5 during 2001-2065. The climatology, plotted in black, is the CMIP5 multi-model average of 1981-2000 from the historical runs and the future projection in (a), plotted in thick red, is the sum of the climatology and the linear response from 2001 to 2099 in the RCP8.5 scenario, similarly for (b)(c). Statistically significant responses at the 90% level, are circled.

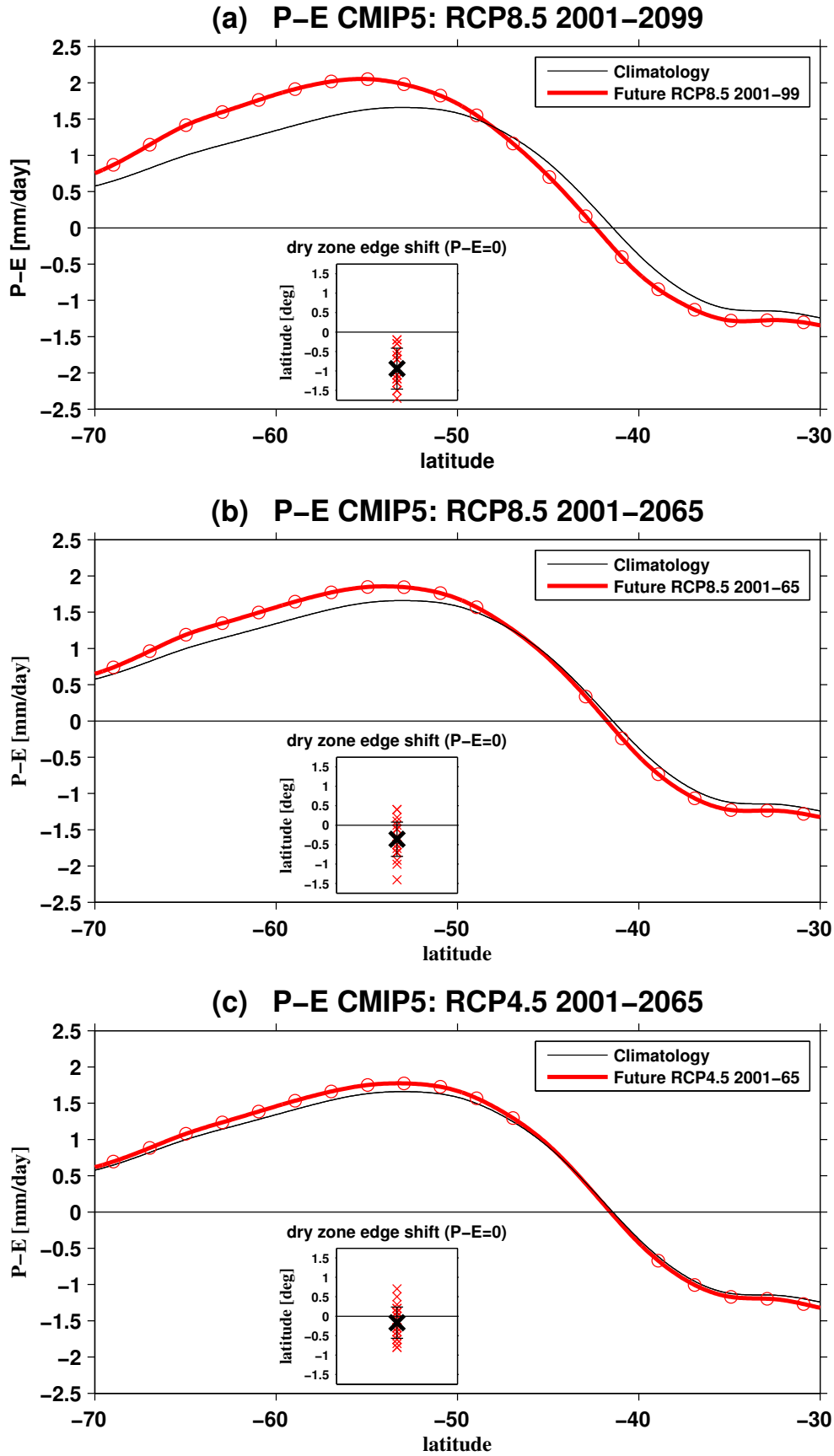


FIG. 2. Same as Fig. 1 except for precipitation minus evaporation ($P - E$). In the inset plot, the latitudinal shift of the subtropical dry zone edge, which is measured by the zero crossing of $P - E$, is plotted in red cross for each model and in thick black cross for multi-model average. Bar shows one standard deviation of the multi-model results.

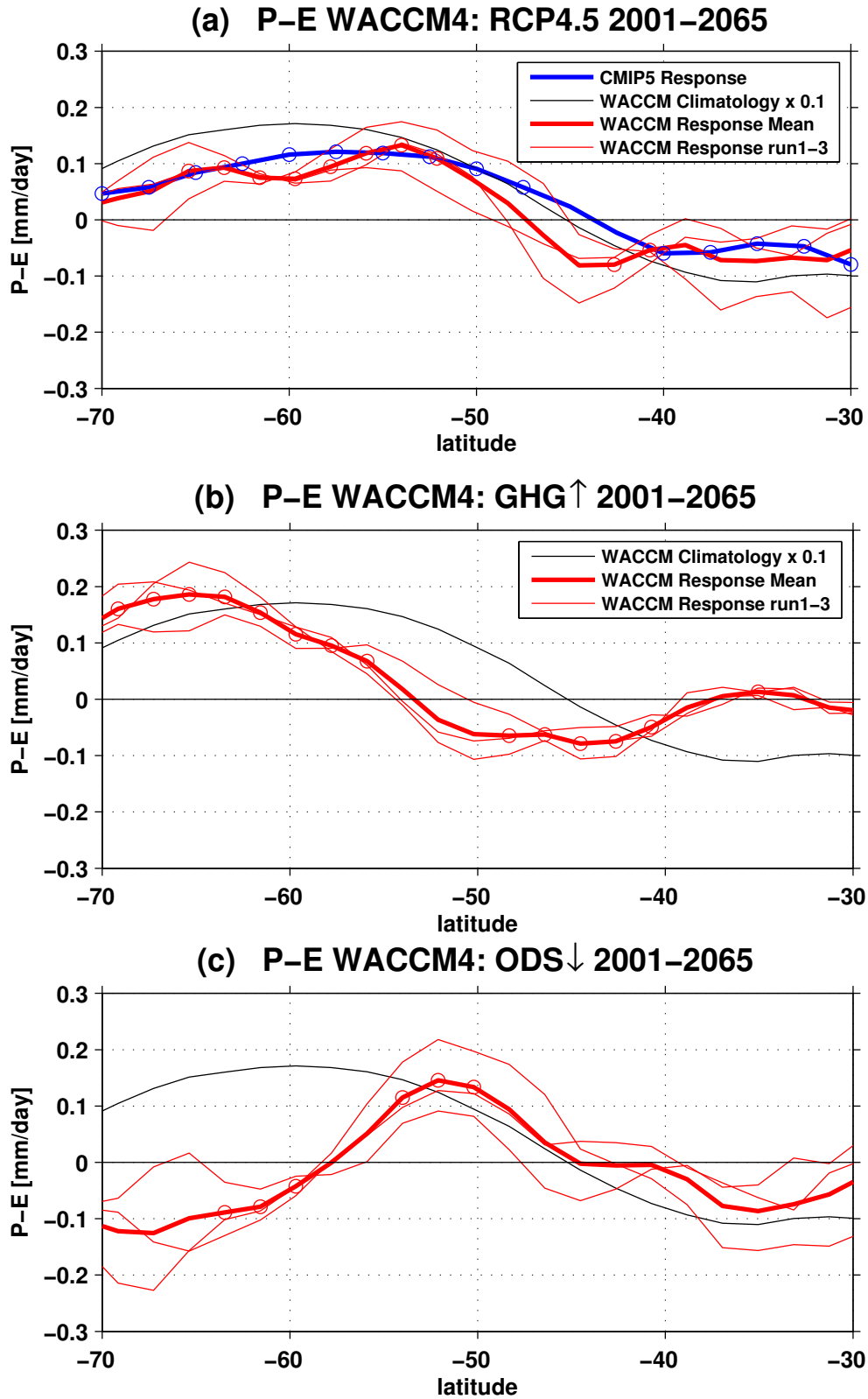


FIG. 3. The linear trend in zonal mean $P - E$ in austral summer (DJF) during 2001-2065 for (a) the RCP4.5 scenario, (b) GHG \uparrow experiment, and (c) ODS \downarrow experiment from the WACCM4 integrations. Thin black line shows the climatology of $P - E$ during 1981-2000 from the WACCM4 historical integrations, divided by a factor of 10. Thick red line shows the linear trend of $P - E$ during 2001-2065 in average of three ensemble runs and thin red line shows the response from individual run. Thick blue line shows the CMIP5 multi-model averages during 2001-2065. Statistically significant responses, at the 90% level, are circled.

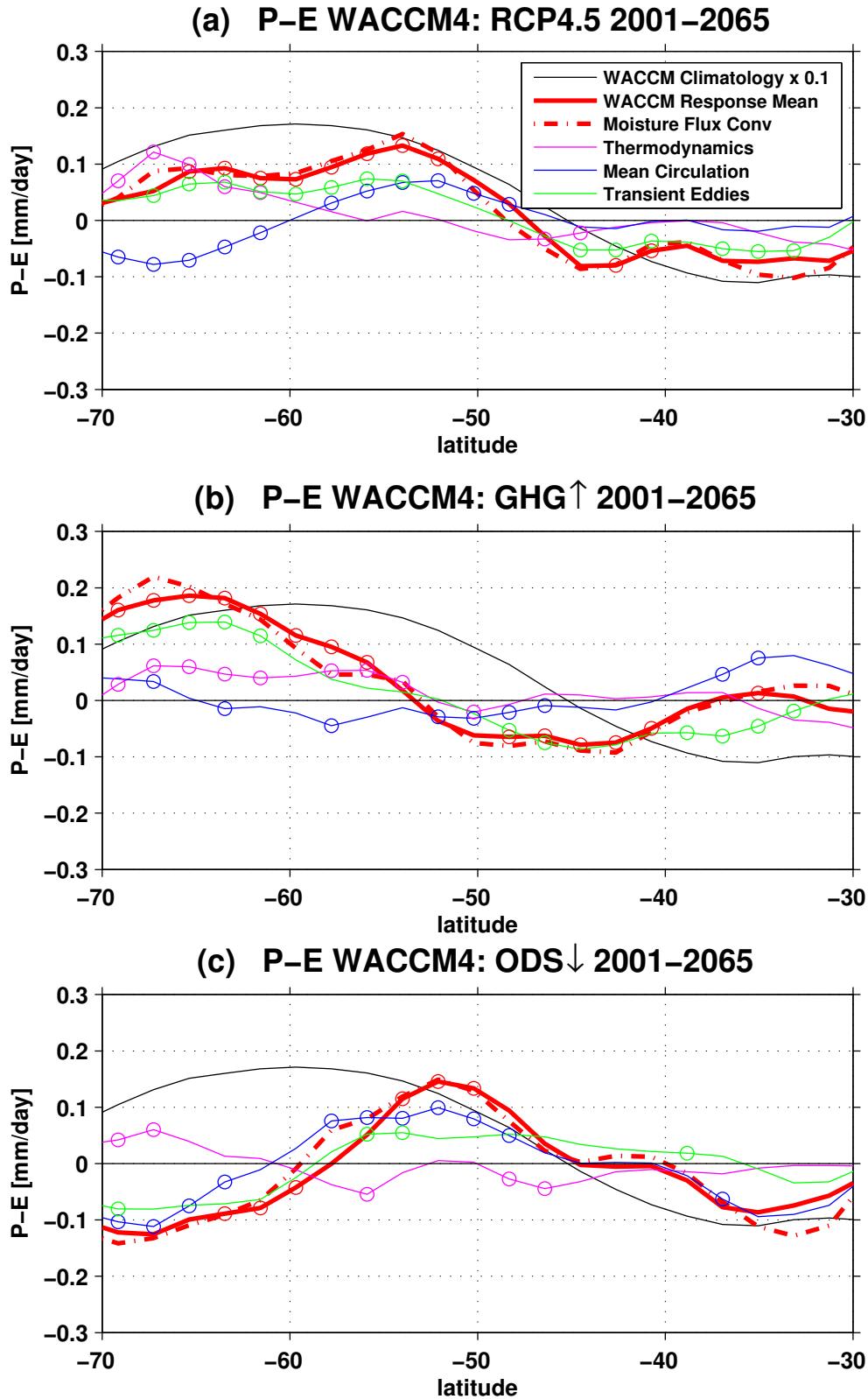


FIG. 4. The WACCM4 moisture budget analysis for the linear trend in zonal mean $P - E$ in DJF for (a) the RCP4.5 scenario, (b) GHG \uparrow experiment, and (c) ODS \downarrow experiment. The 1981-2000 average of $P - E$, divided by a factor of 10, is plotted in thin black as a reference for climatology, and the linear trend of $P - E$ during 2001-2065 is plotted in thick red. The sum of the thermodynamic (magenta), mean circulation dynamic (blue), and transient eddy moisture flux convergence (green) components is denoted by 'moisture flux conv' and is plotted in thick dashed-dotted red line.

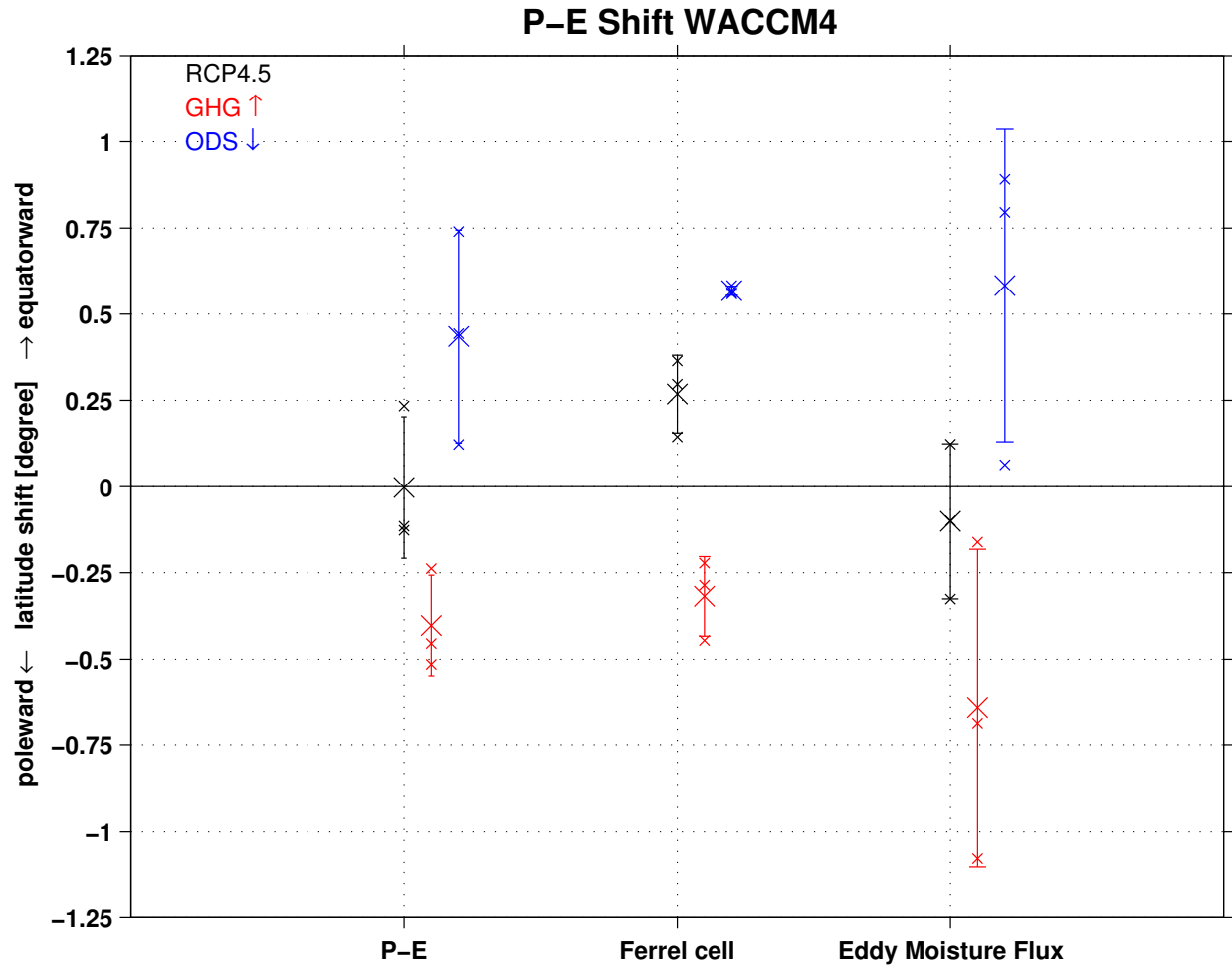


FIG. 5. The latitudinal shift of $P - E$, the Ferrel cell and the transient eddy moisture flux in DJF during 2001-2065. Black indicated the RCP4.5 scenario, red the GHG \uparrow experiment, and blue the ODS \downarrow experiment. Large crosses show ensemble averages; small crosses show individual ensemble members; bars show one standard deviation for each ensemble.

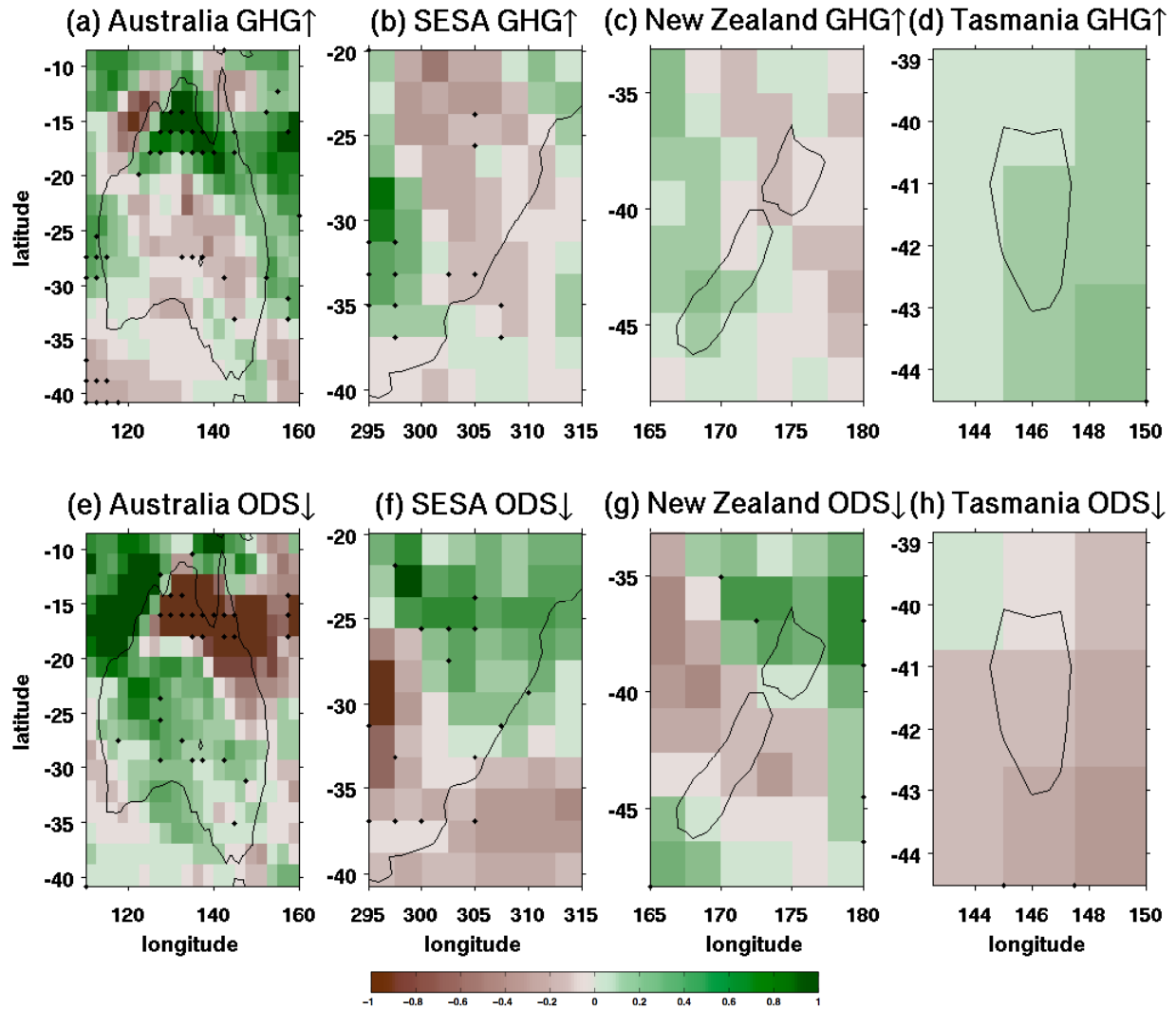


FIG. 6. The linear trend in $P - E$ (in unit of [mm/day]) in DJF during 2001-2065 in (a)(e) Australia, (b)(f) South Eastern South America (SESA), (c)(g) New Zealand, and (d)(h) Tasmania in the GHG \uparrow (top) and ODS \downarrow (bottom) experiments. Statistically significant responses, at the 90% level, are dotted.